Geophysical Research Letters

RESEARCH LETTER
10.1029/2020GL086986

Key Points:
- *P*-wave amplitudes reduce at the onset of preseismic creep for laboratory earthquakes
- The size and onset of amplitude precursors scale with lab earthquake size and fault slip rate
- The microphysical mechanisms responsible for amplitude precursors are similar for the spectrum of fault slip modes

Supporting Information:
- Supporting Information S1

Correspondence to:
S. Shreedharan,
srisharan@psu.edu

Citation:
Shreedharan, S., Bolton, D. C., Rivière, J., & Marone, C. (2020). Preseismic fault creep and elastic wave amplitude precursors scale with lab earthquake magnitude for the continuum of tectonic failure modes. *Geophysical Research Letters*, *46*. https://doi.org/10.1029/2020GL086986

Received 6 JAN 2020
Accepted 3 MAR 2020
Accepted article online 5 MAR 2020

Preseismic Fault Creep and Elastic Wave Amplitude Precursors Scale With Lab Earthquake Magnitude for the Continuum of Tectonic Failure Modes

Srisharan Shreedharan[1], David Chas Bolton[1], Jacques Rivière[2], and Chris Marone[1]

[1]Department of Geosciences, Pennsylvania State University, University Park, PA, USA, [2]Department of Engineering Science and Mechanics, Pennsylvania State University, University Park, PA, USA

Abstract Tectonic faults fail in a continuum of modes from slow earthquakes to elastodynamic rupture. Precursory variations in elastic wavespeed and amplitude, interpreted as indicators of imminent failure, have been observed in limited natural settings and lab experiments where they are thought to arise from contact rejuvenation and microcracking within and around the fault zone. However, the physical mechanisms and connections to fault creep are poorly understood. Here we vary loading stiffness during frictional shear to generate a range of slip modes and measure fault zone properties using transmitted elastic waves. We find that elastic wave amplitudes show clear changes before fault failure. The temporal onset of amplitude reduction scales with lab earthquake magnitude and the magnitude of this reduction varies with fault slip. Our data provide clear evidence of precursors to lab earthquakes and suggest that continuous seismic monitoring could be useful for assessing fault state and seismic hazard potential.

Plain Language Summary Earthquakes in nature can occur slowly, over many days, or rapidly within a few seconds or minutes. In a few cases geoscientists have reported, in hindsight, "precursory" changes in seismic velocities, groundwater levels, and elastic wave attenuation that occurred prior to earthquakes. The ability to robustly identify these signals and accurately attribute them to imminent earthquakes could have a profound effect on our hazard preparedness, particularly for coastal communities where tsunamis occur. Here we study lab earthquakes and use acoustic pulses to image the faults. We show that elastic wave amplitude decreases systematically before failure, providing a clear precursor to failure. The magnitude of this lab earthquake precursor is related to the amount of pre-earthquake fault slip during both slow and fast laboratory earthquakes.

1. Introduction

Earthquake prediction has been a long-standing goal in seismology (Dieterich, 1978; Geller, 1997; Hough, 2016; Rikitake, 1968; Scholz et al., 1973). Part of the difficulty is that without advanced knowledge of an impending earthquake's location, one cannot focus efforts to search for so called precursor-temporal changes in rock (or other) properties prior to failure. However, precursory variations in seismic velocity and amplitude anomalies have been observed in some cases (Crampin et al., 1984; Malagnini et al., 2019; Niu et al., 2008; Whitcomb et al., 1973) and lab work suggests that they might occur for the full spectrum of earthquake failure modes, from slow slip to elastodynamic earthquakes (Kaproth & Marone, 2013; Main & Meredith, 1989; Scuderi et al., 2016). Generally, precursors in nature are thought to arise from pore fluid-modulated variations in effective modulus of fault zones (Sammonds et al., 1992; Yamashita & Tsutsumi, 2018). Precursory seismic amplitude variations, likely related to preslip, have also been observed in limited experiments on sheared rock discontinuities (Chen et al., 1993; Hedayat et al., 2014, 2018). Moreover, recent experimental studies have used premonitory acoustic emission (AE) signals to predict lab earthquake failure times (Hulbert et al., 2019; Rouet-Leduc et al., 2017). Here we address the physical mechanisms responsible for precursors to laboratory earthquakes and focus in particular on the evolution of fault zone elastic properties as imaged by transmitted wave amplitudes.

Active and passive seismic monitoring techniques have proved promising particularly in the realm of reservoir monitoring (Lumley, 2001; Zhu et al., 2019), field studies of postseismic healing (Brenguier et al., 2008), and laboratory studies of fault frictional state (Nagata et al., 2008; Shreedharan et al., 2019; Yoshioka & Iwasa, 2006) and coseismic energy release (Aichele et al., 2018; Latour et al., 2013). The use of acoustic

amplitude (or acoustic transmissivity [AT]; see Supporting Information S1) is particularly appealing here since it has been demonstrated from theory and experiments (Kendall & Tabor, 1971; Kilgore et al., 2017; Nagata et al., 2008; Pyrak-Nolte et al., 1990; Saltiel et al., 2017; Shreedharan et al., 2019) that AT across frictional interfaces is related to the stiffness and size of asperity contact junctions participating in shear. Specifically, AT scales with fault normal stress and healing time and inversely with slip rate during steady-state shear on experimental faults (Ryan et al., 2018; Shreedharan et al., 2019). These scaling relationships arise naturally as a result of the relationship between AT and asperity stiffness. Therefore, studying *P*-wave amplitudes enables us to directly study the microscale physics that control the temporal variations in precursors to laboratory earthquakes. However, whether resolvable precursory signals in AT can be used to monitor the seismogenic state of tectonic faults remains unclear, although theoretical considerations dictate that it should be feasible for faults of nominal strength 25–100 MPa and survey frequencies of 1–100 Hz (Kame et al., 2014).

Here we study elastic waves propagating through frictional interfaces during the full laboratory seismic cycle of loading and failure. We observe preseismic variations in AT linked to preslip and demonstrate that these precursors vary systematically with fault slip rate and earthquake magnitude. Our results allow us to link AT and asperity size and indicate that precursors are a likely outcome of contact area reduction arising from increasing local fault slip rate during a preparatory phase prior to failure.

2. Methods

Our experiments were carried out on the biaxial shear apparatus in a double direct-shear (DDS) configuration in the Penn State Rock Mechanics laboratory (Figure 1a). The apparatus was used to apply normal and shear loads in the horizontal and vertical directions using two hydraulic pistons. Direct current displacement transducers were mounted on the horizontal and vertical pistons (inset to Figure 1a) for far-field normal and shear displacement measurements. In addition, we attached a direct current displacement transducers to the central shearing block and referenced it to the base of the DDS configuration to measure true fault slip. All experiments were performed at a normal stress of 10 MPa and a far-field shear rate of 11 μm/s.

We sheared rough surfaces (5×5 cm^2) of Westerly granite that were coated with thin layers of quartz powder (median grain size of 10.5 μm) to simulate frictional wear and fault gouge. Gouge layers weighed ~0.25 g and were ~250 μm thick prior to the application of normal load. The granite surfaces were roughened with #60 grit (root-mean-square roughness ~20 μm). During shear in our experiments, the gouge layers were comparable in thickness to the maximum surface roughness, causing direct interaction between fault surfaces and wear (Figure S1 in the supporting information).

In contrast to previous experimental works (e.g., Leeman et al., 2016; Scuderi et al., 2016) where the continuum of slip modes was generated by varying the normal stress on the sample, we generated the spectrum of failure modes by varying the machine loading stiffness using acrylic springs of different cross-sectional areas in series with the shear loading piston. This approach eliminates the possibility that differences in normal stress and in turn frictional contact area and ultrasonic amplitudes (Shreedharan et al., 2019) caused the effects we observe.

Active ultrasonic measurements were performed using broadband (~0.02–2 MHz) lead-zirconate (PZT) p-polarized ultrasonic transducers embedded in steel plates coupled to the DDS configuration using molasses. In this study, we use the largest peak-to-peak amplitude within the first 5 μs for ultrasonic data analyses (Figure 1a, yellow waveform). This wavelet represents the transducer response to the first arrival rather than the *P*-wave coda used by previous studies (eg. Scuderi et al., 2016; Singh et al., 2019), which represents accumulated effects of multiple reflections through frictional interfaces and the bulk (Figure 4 in Tinti et al., 2016). For more detailed experimental methods, we refer readers to Shreedharan et al. (2019) and Supporting Information S1.

3. Results

We sheared rough surfaces of Westerly granite decorated with a thin coating of quartz powder to simulate earthquake fault zones. We monitored stresses, fault displacements, and fault slip rate (Figure 1) while conducting continuous ultrasonic monitoring for a range of fault slip modes, slip velocities, and stress drops

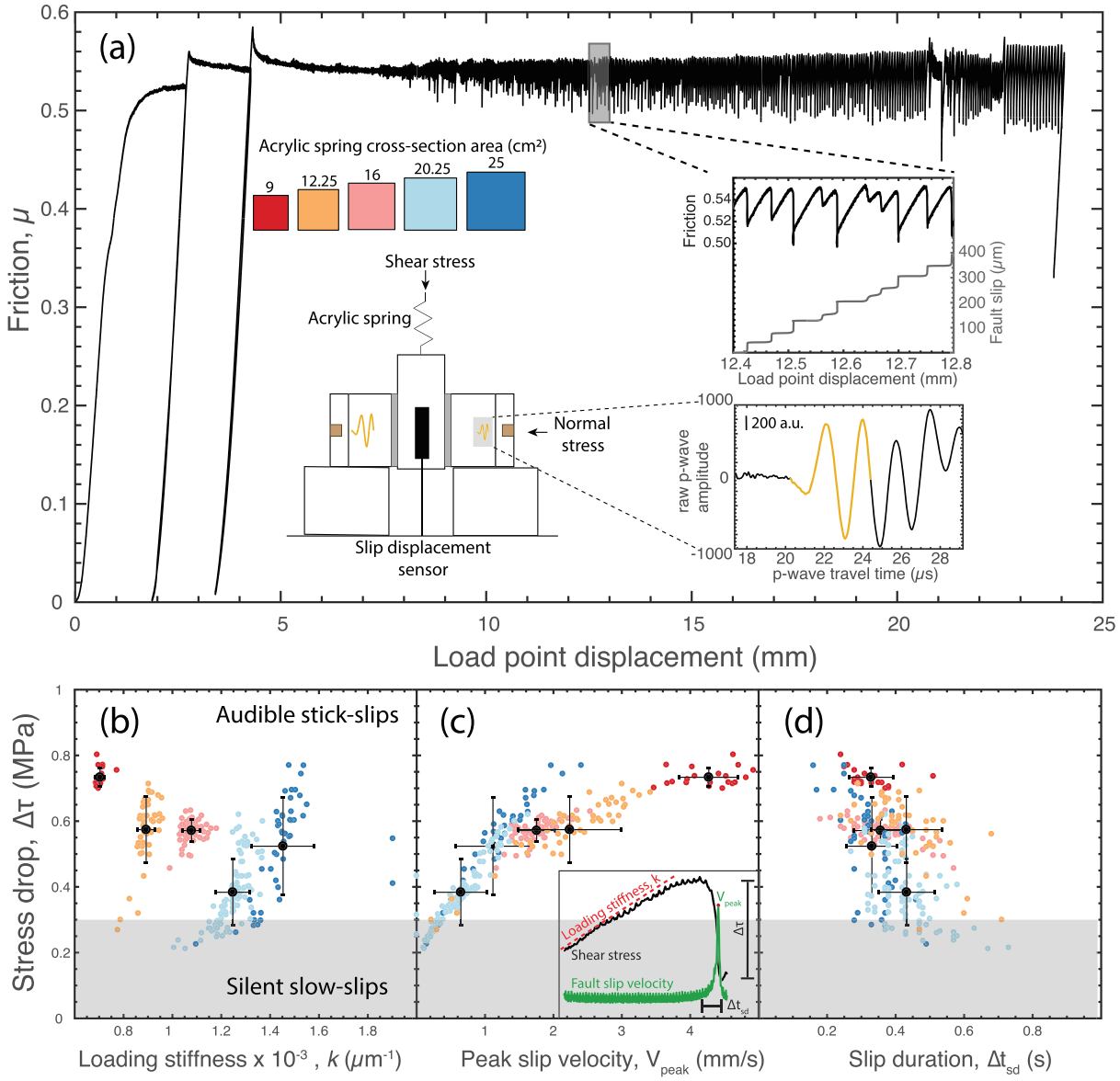

Figure 1. The spectrum of fault slip modes generated by modifying the acrylic spring cross-sectional area (see inset). (a) Friction-displacement for a representative experiment shows the transition from stable sliding to stick-slip behavior after approximately 7 mm shear. Two unload-reload cycles are performed at ~2 and ~4 mm shear displacement. Left (bottom) inset shows a schematic of the double-direct shear setup with ultrasonic monitoring and slip sensor. Middle inset shows a typical ultrasonic pulse passing through the frictional interfaces with the analyzed peak-to-peak amplitudes highlighted in yellow. Right inset shows a sequence of period-doubling stick-slips and associated fault slip. (b) Static stress-drops expressed as a function of elastic loading stiffness show an inverse trend. Colors denote different spring sizes shown in (a). The black dots represent mean values, and the error bars represent 1 standard deviation. (c) Peak slip velocity increases with higher stress-drops and (d) higher stress-drops are associated with lower coseismic slip durations. In b–d, the gray region denotes that silent slow laboratory earthquakes and stick-slip datasets correspond to events in the range of 18–21 mm.

(refer to Table S1 in the supporting information for boundary conditions). We maintained constant frictional contact area and normal stress, which have a nontrivial effect on AT (Shreedharan et al., 2019). Figure S2 shows the effect of varying spring cross-sectional area on loading stiffness. Generally, the loading stiffness increases linearly with cross-sectional area. We observe a transition from stable sliding to quasi-dynamic and subsequently repetitive stick-slips after approximately 8–10 mm of shear (Figure 1a). Our experiments show consistent results including, for some conditions, period-doubling (Inset to Figure 1a) behavior with alternating slow and fast stick-slips, likely due to interactions between the gouge layers and the rough frictional interface of the granite. This observation is consistent with period-doubling observed in

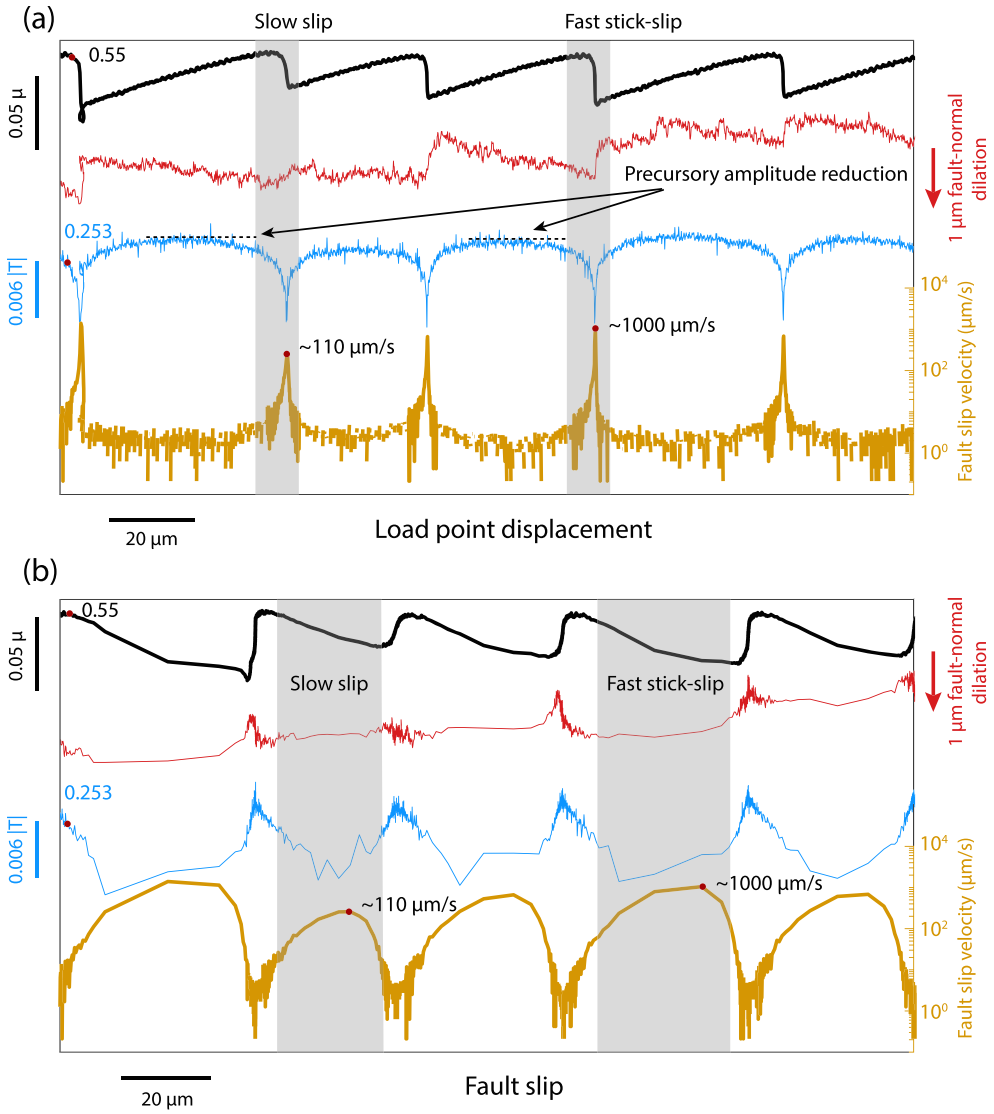

Figure 2. Variation of fault zone dilation, slip rate, and acoustic transmissivity, $|T|$, during stick-slips. The gray boxes denote the coseismic slip phase of a slow and fast slip event. (a) Friction drops, fault zone dilation, fault slip rate, and elastic amplitudes are shown as functions of far-field imposed loading rate. Slow stick-slips are characterized by smaller stress drops than fast stick-slips for a given set of boundary conditions. During the coseismic slip stage, the fault zone compacts, slip rate accelerates, and elastic amplitudes attain a minimum value. Note that slow-slip events are also characterized by smaller peak slip velocities than faster ruptures. The preseismic reduction in amplitudes occurs during the interseismic strain accumulation phase of the stick-slip event. (b) The fault zone attributes in (a) expressed as functions of measured fault slip. Elastic amplitudes and fault zone dilation reach their respective minimum values during the maximum strain release rate portion of the coseismic stress drop. Simultaneously, the fault slip rate reaches its maximum value.

numerical simulations (Gu et al., 1984), in friction experiments when the loading stiffness is close to the critical weakening rate (Leeman et al., 2016; Scuderi et al., 2016) and in nature, along the San Andreas fault (Veedu & Barbot, 2016).

We report measurements of stress drop, peak slip velocity, slip duration, and the effective machine loading stiffness for each stick-slip event (Figure 1). Following Leeman et al. (2016, 2018), we classify slow laboratory earthquakes as the instabilities without audible coseismic energy radiation. In our experiments, slow earthquakes have stress drops of 0.3 MPa or less, maximum peak slip velocities of 300 μm/s, and coseismic durations >0.5 s. Consistent with previous observations (Ide et al., 2007; Leeman et al., 2016; Peng & Gomberg, 2010; Scuderi et al., 2016), slow-slip events have consistently smaller stress drops than dynamic stick-slip instabilities. Additionally, stress drops are negatively correlated with loading stiffness, with the more

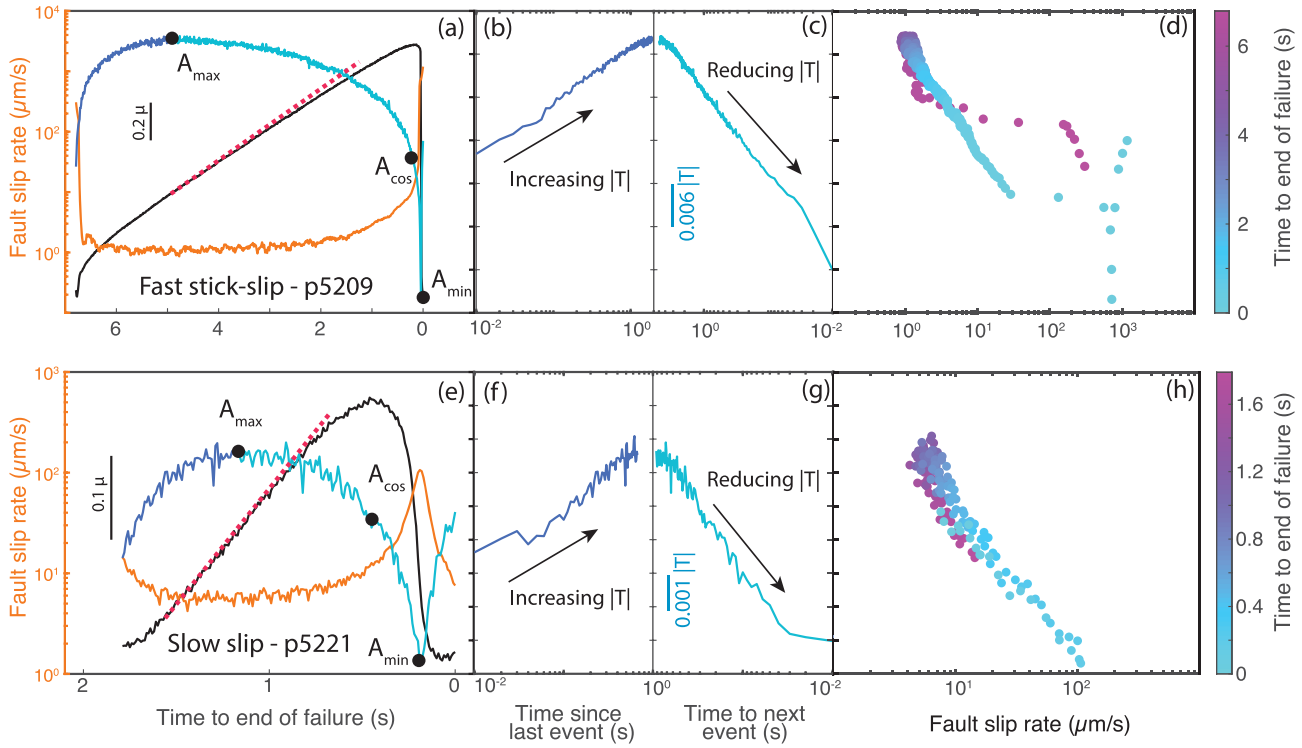

Figure 3. The relationship between precursory amplitude variation and fault slip rate for (panels a–d) slow and (panels e–h) fast laboratory earthquakes. Panels (a) and (e) show friction (black), slip rate (green), and *P*-wave amplitude (purple) evolution for a representative fast and slow laboratory earthquakes, respectively. Note the short slip duration and large friction drop for the fast slip versus the longer transient slip duration for the slow slip. The dashed lines show the loading stiffness of the stick-slip instability. Elastic amplitudes begin to reduce at the onset of inelastic loading and continue to decrease throughout the coseismic slip phase. Panels (b) and (f) show the increasing limb of preseismic amplitudes expressed versus time since previous event on a logarithmic scale. The log-linear relationship of the increasing limb between amplitude and time demonstrates fault healing via contact area increase. While panels (c) and (g) show the reduction in amplitudes from interseismic peak to coseismic minimum, expressed as a function of time until fault failure. Panels (d) and (h) show the elastic amplitudes as a function of slip rate and colored with reference to time to failure of the next slip event. Elastic amplitudes vary log-linearly with fault slip rate. Amplitudes reduce at the onset of preseismic fault slip (see a) and continue to reduce at the same rate until they attain a minimum value during the coseismic slip stage.

compliant system producing larger instabilities (Figure 1b). Earthquake stress drops also increase with increasing peak coseismic slip velocities (Figure 1c) and decrease with higher coseismic slip durations (Figure 1d).

A representative set of stick-slips and their associated mechanical and ultrasonic attributes are shown in Figure 2, with Figures 2a and 2b expressing the instabilities as functions of the imposed far-field shear displacement rate and fault slip rate, respectively. We measure the coefficient of friction (hereafter referred to as friction) as the ratio of fault zone shear and normal stresses. Within the period-doubling space, slow instabilities have peak slip velocities of ~100 μm/s and fast elastodynamic events have peak slip rates of ~1 mm/s, representing an order of magnitude increase in peak slip rate (Figure 2a). Observations of fault normal displacement indicate that the faults undergo dilation during the interseismic period (linear-elastic loading phase), begin to compact prior to failure, and undergo rapid compaction during coseismic failure as the fault slip rate reduces to near zero and the fault locks up (Figure 2b). This indicates that compaction and reduced postseismic slip rate could work in concert to enhance fault healing, by increasing the number and size of frictional contact junctions (Yasuhara et al., 2005). The AT first increases during elastic loading and then decreases prior to failure for both slow and fast slip events (Figure 2a). Interestingly, the onset of preseismic AT reduction also marks the onset of inelastic fault creep and an increase in fault slip rate. That is, the *P*-wave amplitudes decrease once the fault begins to unlock and inelastic loading occurs (Figure 2a). Subsequently, the amplitudes reduce to a minimum during the coseismic slip phase when the fault reaches its peak slip rate (Figure 2b).

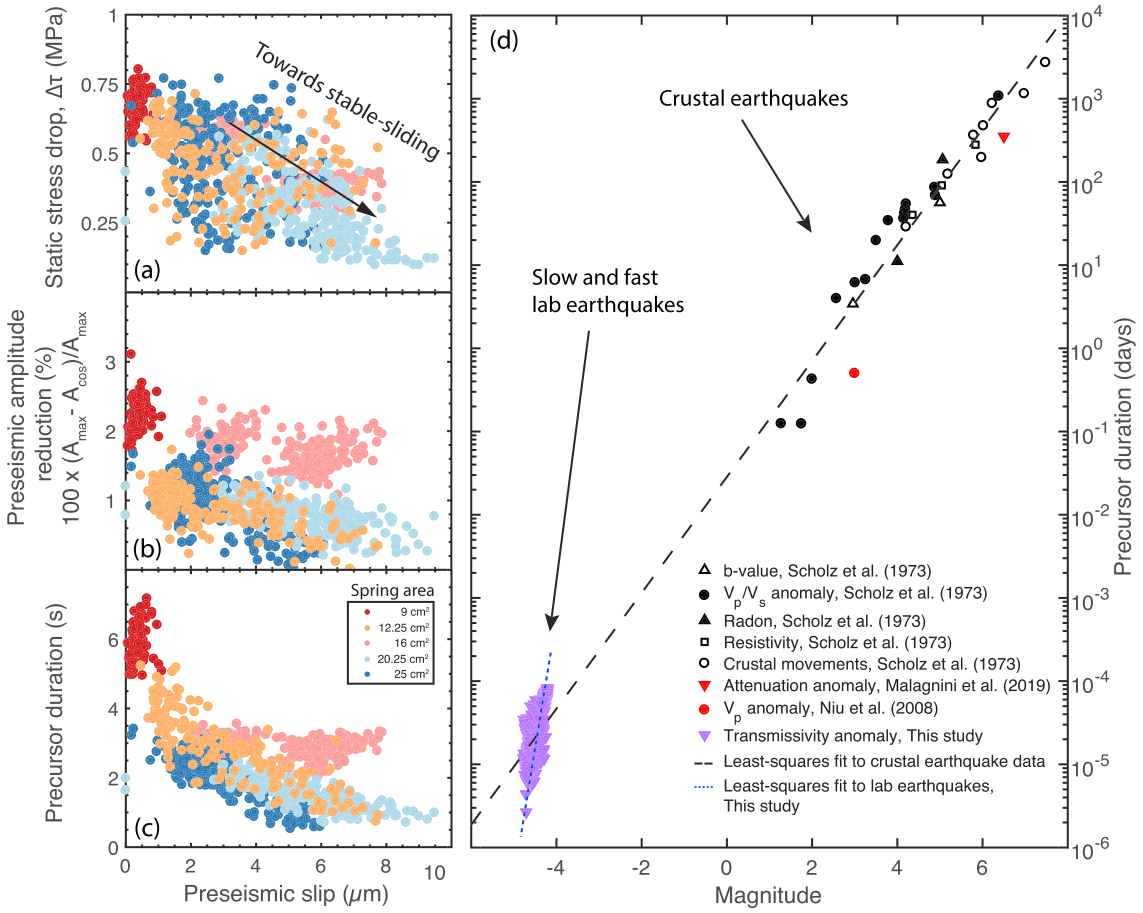

Figure 4. Relationship between preslip, precursors and earthquake size. (a) Static stress-drop and preseismic slip are inversely related to each other for a given normal stress and imposed loading rate. (b) Preseismic amplitude reduction scales inversely with preseismic slip, and thus, is directly correlated to the magnitude of the slip event. (c) Preseismic amplitudes reduce earlier in the interseismic period for slip events with smaller amounts of preslip and larger stress drops. (d) Onset of precursors increases as a function of magnitude of subsequent earthquakes across several scales.

4. Discussion

Taken together, the variations in AT and fault slip during our laboratory earthquakes indicate that the precursory variations in AT quantitatively track fault slip rate (Figure 3). This observation is consistent with the long-held assertion that preslip could dictate the characteristics of earthquake precursors in nature (Acosta et al., 2019; Chen et al., 1993; Dieterich, 1978; Hedayat et al., 2014; Scholz, 2019). Broadly, variations in AT observed in our experiments can be classified into two preseismic stages (Figures 3a and 3e): first, the increase in AT during the linear-elastic loading phase of the interseismic period, which follows fault slip deceleration and subsequent lock-up after failure (Figures 3a and 3e). During the linear-elastic loading phase, AT increases logarithmically with time (Figures 3b and 3f), consistent with observations of fault healing in friction experiments (Dieterich, 1972; Ryan et al., 2018; Shreedharan et al., 2019) and in nature (Brenguier et al., 2008; Marone, 1998a, 1998b). We interpret this increase in AT as an increase in the specific stiffness (see Figure S3 and Hedayat et al., 2014) and strength of microscopic contact junctions that make up the granular interface, either via an increase in the number or size (or both) of asperities during the "healing" phase (Li et al., 2011; Shreedharan et al., 2019).

The second stage is marked by the onset of inelastic fault creep prior to failure for fast (Figure 3a) and slow slip events (Figure 3e) and begins when AT has reached a peak value. This systematic transition from first to second stage makes transmittivity a reliable precursor to failure. Transmittivity reduces continuously during the second stage until the fault reaches its minimum shear stress during coseismic failure, with the reduction being linear in log-time (Figures 3c and 3g).

During coseismic fault slip, the AT attains a minimum coincident with peak fault slip rate. The maxima and minima attained by fault slip and AT, respectively, also correspond to the peak frictional unloading rate. It is interesting to note that we observe no break in slope in the amplitude-time variation during the transition from preseismic to coseismic slip (Figures 3c and 3e). This indicates that the contact-scale mechanics controlling slip behavior may be similar for both preseismic and coseismic slips. The two-stage nature of the AT precursor is consistent with previous works that documented an elastic wave velocity precursor that was controlled by fault zone preslip (Kaproth & Marone, 2013; Scuderi et al., 2016). Note the clear inverse relationship between AT and fault slip rate at various stages of the laboratory seismic cycle (Figures 3d and 3h; see also Figure S3 for a phase-plane representation of the data). Preseismic AT variations documented in our experiments could be indicative of cascading, predictable failure (Hulbert et al., 2019). Thus, our results suggest that continuous seismic monitoring may be used in natural settings to gather insight into imminent fault failure, assuming a nearly linear scaling of underlying mechanisms in space and/or time. However, we note that extrapolating our results to field scales may not be straightforward. In particular, preslip on natural faults is often small and may not always be resolvable (e.g., Amoruso & Crescentini, 2009). Additionally, at low strain rates approaching those experienced by natural faults, laboratory AE foreshock precursors have been observed to become temporally shorter, occurring closer to failure (McLaskey & Kilgore, 2013; Ojala et al., 2004; Selvadurai & Glaser, 2015), although the relationship between the mechanics of AE production and AT is poorly known.

Figure 4 shows the relationship between preseismic slip, coseismic stress drops, and precursory amplitude reduction prior to failure. Preseismic slip is calculated here as the total slip undergone, as measured by the slip displacement sensor (Figure 1a), between the interseismic minimum shear stress and peak shear stress just before failure. Our results indicate a robust relationship between AT variations and precursory slip (Figure 4). These observations are consistent with previous AE studies that have suggested that microscopic slip is related to the increase in AE activity prior to laboratory stick-slips (Johnson et al., 2013).

Preslip has been shown to vary with effective normal stress, loading rate, and fault zone thickness (Acosta et al., 2019; Anthony & Marone, 2005; Leeman et al., 2018; Scuderi et al., 2015). However, the effect of loading stiffness alone on preseismic slip is not well documented. Our observations show that preslip varies inversely with stress drop magnitude (Figure 4a) for the range of stiffnesses explored in this study. In other words, faults experiencing higher preslip release some of the accumulated strain energy via preseismic sliding resulting in a lower coseismic stress drop magnitude (Cattania & Segall, 2019). This is consistent with the theory of time-dependent healing (Dieterich, 1978; Marone, 1998b) within the framework of rate-and-state friction, where higher healing is associated with an increase in subsequent seismic magnitude via an increase in real area of contact at asperity junctions. Specifically, as we increase loading stiffness, we observe a transitioning to stable sliding, representing infinite preslip.

Simultaneously, we calculate the reduction in preseismic AT as the percent reduction from peak AT during elastic loading (A_{max}) to the AT at peak friction prior to failure (A_{cos}), referenced against the peak AT (Figures 3 and 4b). We observe that the precursory AT variations are systematically higher when the fault experiences little to no preseismic slip (e.g., largest slip events). Conversely, the smallest precursory AT signatures are associated with the highest preseismic slip and smaller magnitude slip events. This indicates that the fault locks up more (i.e., experiences a lower interseismic minimum slip rate) preceding ruptures with large stress drops. This allows for a higher magnitude of healing and longer healing times preceding larger coseismic stress drops. Thus, while the onset of the precursory AT reduction is related to the temporal onset of preslip, the size of the AT precursor is intimately related to the maximum slip rate excursion experienced by the fault. This is apparent in Figures 3a and 3d when the interseismic AT increases rapidly for ~2 s for the fast rupture, whereas it increases more gradually for ~0.5 s when the strain accumulation culminates in a slow earthquake (Figure 3e). Finally, our observations of the precursory AT variation indicate that the onset of the amplitude precursor occurs earlier in the seismic cycle when the fault undergoes less macroscopic preslip and the onset is delayed as the fault undergoes more preslip (Figure 4c). The fault achieves lower slip rates earlier in the interseismic period preceding larger instabilities, and AT is related to the logarithm of the fault slip rate. Hence, the onset of small microslip precursors produces large, resolvable precursory amplitude signals earlier in the interseismic period preceding large laboratory earthquakes.

Our experiments show preseismic AT reductions of 2–3% for stress drops of ~0.75 MPa (Figure 4). However, extrapolating these values to tectonic faults is not straightforward. First, field surveys involving fault zone monitoring generally utilize frequencies in the range of 1–1,000 Hz (Niu et al., 2008), which are significantly lower than those used in our study. Additionally, field surveys focus on the reflection coefficient rather than its transmission counterpart. Kame et al. (2014) demonstrate that faults in nature have characteristic frequencies of 1–100 Hz. In such cases, they show that faults of strength 25–100 MPa, exhibiting coseismic stress drops of ~15 MPa, should undergo an ~5.5% change in the reflection coefficient, which is consistent with our observation of ~2% reduction in the AT for stress drops of 0.75–1 MPa.

We also cast the temporal onset of transmissivities in the context of natural earthquakes by converting coseismic slip into seismic moment (Acosta et al., 2019). We assume a shear modulus of 3 GPa for quartz gouge (Kenigsberg et al., 2019) and that the entire fault area (25 cm^2) ruptures, which is reasonable when the fault patch is smaller than a critical nucleation length (McLaskey & Lockner, 2014). Our results (Figure 4d) fall remarkably close to the scaling between onset of precursors and eventual earthquake size reported by Scholz et al. (1973), as well as more recent examples of potential precursors to natural earthquakes. However, the scaling relationship for our data (dotted line, Figure 4d) has a significantly higher slope. This could be due to different mechanisms operating in our experiments (preslip-driven precursors) compared to mechanisms postulated in nature (dilatancy-diffusion and fluid-modulated precursors). We also do not rule out the possibility that observations of precursors in nature suffer from retrospective selection bias arising out of random fluctuations in a Poisson process (Main et al., 2012). Additionally, there is a general lack of observations of robust precursors for earthquakes in nature (Bakun et al., 2005; Jordan et al., 2011). Hence, more focused studies, including incorporating pore pressure, may be necessary to address whether similar microphysical processes operate in concert to produce precursors over multiple scales.

5. Conclusions and Future Directions

We report on the evolution of fault zone elastic properties throughout the laboratory seismic cycle. The transmitted wave amplitude robustly tracks precursory fault slip prior to both slow and fast laboratory earthquakes. Our observations indicate that elastic wave amplitudes are robust precursors to failure that are consistent with and higher resolution than elastic wave velocity precursors. Our data suggest that time-lapse active seismic monitoring of faults in nature could provide critical information pertinent to preslip, foreshocks, and imminent failure. The utility of active seismic monitoring of wave amplitude has been consistently demonstrated in theoretical studies (Kame et al., 2014) and in limited field-based surveys such as those related to CO_2 injection and storage (Arts et al., 2004; Zhu et al., 2019). Future research should focus on applying active seismic techniques to monitor fault zones for hazard quantification and mitigation (e.g., Niu et al., 2008). Finally, our results demonstrate the similarity between the microphysical mechanisms operating before slow and fast earthquakes, which has important implications to further our understanding of the mechanics of slow slip and the feedback between the observed spectrum of tectonic slip modes.

Acknowledgments
We thank Ake Fagereng, Ian Main, Paul Selvadurai, and an anonymous reviewer for their thorough reviews. Technical assistance from laboratory manager Steve Swavely is gratefully acknowledged. This study was supported by NSF-EAR1520760, DOE Office of Basic Energy Science contract DE-SC0017585, and an International Ocean Discovery Program (IODP) Schlanger Fellowship to S. S. Data are available from the PSU Scholarsphere repository (https://doi.org/10.26207/12jy-rw97) or by contacting the corresponding author.

References

Acosta, M., Passelegue, F. X., Schubnel, A., Madariaga, R., & Violay, M. (2019). Can precursory moment release scale with earthquake magnitude? A view from the laboratory. *Geophysical Research Letters*, *46*, 12,927–12,937. https://doi.org/10.1029/2019GL084744

Aichele, J., Catheline, S., Roux, P., Latour, S., & Voisin, C. (2018). Ultrafast ultrasound captures dynamic rupture behavior. In *Proceedings of Meetings on Acoustics 21ISNA* (Vol. 34, no. 1, p. 045044). ASA.

Amoruso, A., & Crescentini, L. (2009). Slow diffusive fault slip propagation following the 6 April 2009 L'Aquila earthquake, Italy. *Geophysical Research Letters*, *36*, L24306. https://doi.org/10.1029/2009GL041503

Anthony, J. L., & Marone, C. (2005). Influence of particle characteristics on granular friction. *Journal of Geophysical Research*, *110*, B08409. https://doi.org/10.1029/2004JB003399

Arts, R., Eiken, O., Chadwick, A., Zweigel, P., Van der Meer, L., & Zinszner, B. (2004). Monitoring of CO2 injected at Sleipner using time-lapse seismic data. *Energy*, *29*(9–10), 1383–1392.

Bakun, W. H., Aagaard, B., Dost, B., Ellsworth, W. L., Hardebeck, J. L., Harris, R. A., et al. (2005). Implications for prediction and hazard assessment from the 2004 Parkfield earthquake. *Nature*, *437*(7061), 969–974. https://doi.org/10.1038/nature04067

Brenguier, F., Campillo, M., Hadziioannou, C., Shapiro, N. M., Nadeau, R. M., & Larose, E. (2008). Postseismic relaxation along the San Andreas fault at Parkfield from continuous seismological observations. *Science*, *321*(5895), 1478–1481.

Cattania, C., & Segall, P. (2019). Crack models of repeating earthquakes predict observed moment-recurrence scaling. *Journal of Geophysical Research: Solid Earth*, *124*, 476–503. https://doi.org/10.1029/2018JB016056

Chen, W. Y., Lovell, C. W., Haley, G. M., & Pyrak-Nolte, L. J. (1993). Variation of shear-wave amplitude during frictional sliding. *International Journal of Rock Mechanics and Mining Sciences & Geomechanics Abstracts*, *30*(7), 779–784. https://doi.org/10.1016/0148-9062(93)90022-6

Crampin, S., Evans, R., & Atkinson, B. K. (1984). Earthquake prediction: A new physical basis. *Geophysical Journal International*, *76*(1), 147–156.

Dieterich, J. H. (1972). Time-dependent friction in rocks. *Journal of Geophysical Research*, *77*(20), 3690–3697.

Dieterich, J. H. (1978). Preseismic fault slip and earthquake prediction. *Journal of Geophysical Research*, *83*(B8), 3940–3948.

Geller, R. J. (1997). Earthquake prediction: A critical review. *Geophysical Journal International*, *131*(3), 425–450.

Gu, J. C., Rice, J. R., Ruina, A. L., & Simon, T. T. (1984). Slip motion and stability of a single degree of freedom elastic system with rate and state dependent friction. *Journal of the Mechanics and Physics of Solids*, *32*(3), 167–196.

Hedayat, A., Haeri, H., Hinton, J., Masoumi, H., & Spagnoli, G. (2018). Geophysical signatures of shear-induced damage and frictional processes on rock joints. *Journal of Geophysical Research: Solid Earth*, *123*, 1143–1160. https://doi.org/10.1002/2017JB014773

Hedayat, A., Pyrak-Nolte, L. J., & Bobet, A. (2014). Precursors to the shear failure of rock discontinuities. *Geophysical Research Letters*, *41*, 5467–5475. https://doi.org/10.1002/2014GL060848

Hough, S. E. (2016). *Predicting the unpredictable: The tumultuous science of earthquake prediction*. Princeton, NJ: Princeton University Press.

Hulbert, C., Rouet-Leduc, B., Johnson, P. A., Ren, C. X., Rivière, J., Bolton, D. C., & Marone, C. (2019). Similarity of fast and slow earthquakes illuminated by machine learning. *Nature Geoscience*, *12*(1), 69.

Ide, S., Beroza, G. C., Shelly, D. R., & Uchide, T. (2007). A scaling law for slow earthquakes. *Nature*, *447*(7140), 76–79. https://doi.org/10.1038/nature05780

Johnson, P. A., Ferdowsi, B., Kaproth, B. M., Scuderi, M., Griffa, M., Carmeliet, J., et al. (2013). Acoustic emission and microslip precursors to stick-slip failure in sheared granular material. *Geophysical Research Letters*, *40*, 5627–5631. https://doi.org/10.1002/2013GL057848

Jordan, T. H., Chen, Y. T., Gasparini, P., Madariaga, R., Main, I., Marzocchi, W., et al. (2011). Operational earthquake forecasting. State of knowledge and guidelines for utilization. *Annals of Geophysics*, *54*(4).

Kame, N., Nagata, K., Nakatani, M., & Kusakabe, T. (2014). Feasibility of acoustic monitoring of strength drop precursory to earthquake occurrence. *Earth, Planets and Space*, *66*(1), 41.

Kaproth, B. M., & Marone, C. (2013). Slow earthquakes, preseismic velocity changes, and the origin of slow frictional stick-slip. *Science*, *341*(6151), 1229–1232.

Kendall, K., & Tabor, D. (1971). An utrasonic study of the area of contact between stationary and sliding surfaces. *Proceedings of the Royal Society of London. A. Mathematical and Physical Sciences*, *323*(1554), 321–340.

Kenigsberg, A. R., Rivière, J., Marone, C., & Saffer, D. M. (2019). The effects of shear strain, fabric, and porosity evolution on elastic and mechanical properties of clay-rich fault gouge. *Journal of Geophysical Research: Solid Earth*, *124*, 10,968–10,982. https://doi.org/10.1029/2019JB017944

Kilgore, B., Beeler, N. M., Lozos, J., & Oglesby, D. (2017). Rock friction under variable normal stress. *Journal of Geophysical Research: Solid Earth*, *122*, 7042–7075. https://doi.org/10.1002/2017JB014049

Latour, S., Voisin, C., Renard, F., Larose, E., Catheline, S., & Campillo, M. (2013). Effect of fault heterogeneity on rupture dynamics: An experimental approach using ultrafast ultrasonic imaging. *Journal of Geophysical Research: Solid Earth*, *118*, 5888–5902. https://doi.org/10.1002/2013JB010231

Leeman, J. R., Marone, C., & Saffer, D. M. (2018). Frictional mechanics of slow earthquakes. *Journal of Geophysical Research: Solid Earth*, *123*, 7931–7949. https://doi.org/10.1029/2018JB015768

Leeman, J. R., Saffer, D. M., Scuderi, M. M., & Marone, C. (2016). Laboratory observations of slow earthquakes and the spectrum of tectonic fault slip modes. *Nature Communications*, *7*, 11104.

Li, Q., Tullis, T. E., Goldsby, D., & Carpick, R. W. (2011). Frictional ageing from interfacial bonding and the origins of rate and state friction. *Nature*, *480*(7376), 233–236. https://doi.org/10.1038/nature10589

Lumley, D. E. (2001). Time-lapse seismic reservoir monitoring. *Geophysics*, *66*(1), 50–53.

Main, I. G., Bell, A. F., Meredith, P. G., Geiger, S., & Touati, S. (2012). The dilatancy–diffusion hypothesis and earthquake predictability. *Geological Society, London, Special Publications*, *367*(1), 215–230.

Main, I. G., & Meredith, P. G. (1989). Classification of earthquake precursors from a fracture mechanics model. *Tectonophysics*, *167*(2–4), 273–283.

Malagnini, L., Dreger, D. S., Bürgmann, R., Munafò, I., & Sebastiani, G. (2019). Modulation of seismic attenuation at Parkfield, before and after the 2004 M6 eearthquake. *Journal of Geophysical Research: Solid Earth*, *124*, 5836–5853. https://doi.org/10.1029/2019JB017372

Marone, C. (1998a). Laboratory-derived friction laws and their application to seismic faulting. *Annual Review of Earth and Planetary Sciences*, *26*(1), 643–696.

Marone, C. (1998b). The effect of loading rate on static friction and the rate of fault healing during the earthquake cycle. *Nature*, *391*(6662), 69.

McLaskey, G., & Lockner, D. A. (2014). Preslip and cascade processes initiating laboratory stick slip. *Journal of Geophysical Research: Solid Earth*, *119*, 6323–6336. https://doi.org/10.1002/2014JB011220

McLaskey, G. C., & Kilgore, B. D. (2013). Foreshocks during the nucleation of stick-slip instability. *Journal of Geophysical Research: Solid Earth*, *118*, 2982–2997. https://doi.org/10.1002/jgrb.50232

Nagata, K., Nakatani, M., & Yoshida, S. (2008). Monitoring frictional strength with acoustic wave transmission. *Geophysical Research Letters*, *35*, L06310. https://doi.org/10.1029/2007GL033146

Niu, F., Silver, P. G., Daley, T. M., Cheng, X., & Majer, E. L. (2008). Preseismic velocity changes observed from active source monitoring at the Parkfield SAFOD drill site. *Nature*, *454*(7201), 204–208. https://doi.org/10.1038/nature07111

Ojala, I. O., Main, I. G., & Ngwenya, B. T. (2004). Strain rate and temperature dependence of Omori law scaling constants of AE data: Implications for earthquake foreshock-aftershock sequences. *Geophysical Research Letters*, *31*, L24617. https://doi.org/10.1029/2004GL020781

Peng, Z., & Gomberg, J. (2010). An integrated perspective of the continuum between earthquakes and slow-slip phenomena. *Nature Geoscience*, *3*(9), 599.

Pyrak-Nolte, L. J., Myer, L. R., & Cook, N. G. (1990). Transmission of seismic waves across single natural fractures. *Journal of Geophysical Research*, *95*(B6), 8617–8638.

Rikitake, T. (1968). Earthquake prediction. *Earth-Science Reviews*, *4*, 245–282.

Rouet-Leduc, B., Hulbert, C., Lubbers, N., Barros, K., Humphreys, C. J., & Johnson, P. A. (2017). Machine learning predicts laboratory earthquakes. *Geophysical Research Letters*, *44*, 9276–9282. https://doi.org/10.1002/2017GL074677

Ryan, K. L., Rivière, J., & Marone, C. (2018). The role of shear stress in fault healing and frictional aging. *Journal of Geophysical Research: Solid Earth*, *123*, 10–479. https://doi.org/10.1029/2018JB016296

Saltiel, S., Selvadurai, P. A., Bonner, B. P., Glaser, S. D., & Ajo-Franklin, J. B. (2017). Experimental development of low-frequency shear modulus and attenuation measurements in mated rock fractures: Shear mechanics due to asperity contact area changes with normal stress. *Geophysics*, *82*(2), M19–M36.

Sammonds, P. R., Meredith, P. G., & Main, I. G. (1992). Role of pore fluids in the generation of seismic precursors to shear fracture. *Nature*, *359*(6392), 228.

Scholz, C. H. (2019). *The mechanics of earthquakes and faulting*. Cambridge, UK: Cambridge University Press. https://doi.org/10.1017/9781316681473

Scholz, C. H., Sykes, L. R., & Aggarwal, Y. P. (1973). Earthquake prediction: A physical basis. *Science*, *181*(4102), 803–810. https://doi.org/10.1126/science.181.4102.803

Scuderi, M. M., Carpenter, B. M., Johnson, P. A., & Marone, C. (2015). Poromechanics of stick-slip frictional sliding and strength recovery on tectonic faults. *Journal of Geophysical Research: Solid Earth*, *120*, 6895–6912. https://doi.org/10.1002/2015JB011983

Scuderi, M. M., Marone, C., Tinti, E., Di Stefano, G., & Collettini, C. (2016). Precursory changes in seismic velocity for the spectrum of earthquake failure modes. *Nature Geoscience*, *9*(9), 695–700. https://doi.org/10.1038/ngeo2775

Selvadurai, P. A., & Glaser, S. D. (2015). Laboratory-developed contact models controlling instability on frictional faults. *Journal of Geophysical Research: Solid Earth*, *120*, 4208–4236. https://doi.org/10.1002/2014JB011690

Shreedharan, S., Rivière, J., Bhattacharya, P., & Marone, C. (2019). Frictional state evolution during normal stress perturbations probed with ultrasonic waves. *Journal of Geophysical Research: Solid Earth*, *124*, 5469–5491. https://doi.org/10.1029/2018JB016885

Singh, J., Curtis, A., Zhao, Y., Cartwright-Taylor, A., & Main, I. (2019). Coda wave interferometry for accurate simultaneous monitoring of velocity and acoustic source locations in experimental rock physics. *Journal of Geophysical Research: Solid Earth*, *124*, 5629–5655. https://doi.org/10.1029/2019JB017577

Tinti, E., Scuderi, M. M., Scognamiglio, L., Di Stefano, G., Marone, C., & Collettini, C. (2016). On the evolution of elastic properties during laboratory stick-slip experiments spanning the transition from slow slip to dynamic rupture. *Journal of Geophysical Research: Solid Earth*, *121*, 8569–8594. https://doi.org/10.1002/2016JB013545

Veedu, D. M., & Barbot, S. (2016). The Parkfield tremors reveal slow and fast ruptures on the same asperity. *Nature*, *532*(7599), 361–365. https://doi.org/10.1038/nature17190

Whitcomb, J. H., Garmany, J. D., & Anderson, D. L. (1973). Earthquake prediction: Variation of seismic velocities before the San Francisco earthquake. *Science*, *180*(4086), 632–635.

Yamashita, T., & Tsutsumi, A. (2018). *Involvement of fluids in earthquake ruptures*. Tokyo, Japan: Springer. https://doi.org/10.1007/978-4-431-56562-8

Yasuhara, H., Marone, C., & Elsworth, D. (2005). Fault zone restrengthening and frictional healing: The role of pressure solution. *Journal of Geophysical Research*, *110*, B06310. https://doi.org/10.1029/2004JB003327

Yoshioka, N., & Iwasa, K. (2006). A laboratory experiment to monitor the contact state of a fault by transmission waves. *Tectonophysics*, *413*(3–4), 221–238.

Zhu, T., Ajo-Franklin, J., Daley, T. M., & Marone, C. (2019). Dynamics of geologic CO_2 storage and plume motion revealed by seismic coda waves. *Proceedings of the National Academy of Sciences*, *116*(7), 2464–2469.

Geophysical Research Letters

Supporting Information for

Preseismic Fault Creep and Elastic Wave Amplitude Precursors Scale with Lab Earthquake Magnitude for the Continuum of Tectonic Failure Modes

Srisharan Shreedharan[1*], David Chas Bolton[1], Jacques Rivière[2], Chris Marone[1]

[1]Dept. of Geosciences, Pennsylvania State University, University Park, PA 16802 USA

[2]Dept. of Engineering Science and Mechanics, Pennsylvania State University, University Park, PA 16802 USA

Contents of this file

Supplementary Item 1

Data Acquisition Parameters

All experiments were conducted at room temperature and a relative humidity of 100% to ensure reproducibility. Mechanical data were acquired using a 24-bit ±10 V analog-to-digital converter at 10 kHz and averaged in real-time to 1000 Hz prior to saving. Ultrasonic half-sinusoidal pulses with a frequency of 500 kHz were transmitted through the frictional interfaces at a rate of 1000 pulses per second. Each received waveform was sampled by a Verasonics high-speed digitizer at 25 MHz for ~80 μs, corresponding to a trace length of 2048 samples.

Generating the Spectrum of Tectonic Failure Modes

Within the framework of frictional slip stability (*Gu et al., 1984*), the transition from stable sliding to unstable stick-slip is a consequence of the interactions between the loading stiffness, k, and the rate of fault weakening with slip, which is given by the critical stiffness, k_c:

$$k < k_c = \frac{\sigma_{eff}(b-a)}{D_c} \quad (1)$$

Here, σ_{eff} is the effective normal stress imposed on the sample, a and b are rate-state friction constants and D_c is a characteristic slip distance. We vary the ratio of k/k_c to generate the full spectrum of slow and fast stick-slips (*Leeman et al., 2016)* by varying the nominal contact area of an acrylic spring in series with the loading column (Inset to Figure 1a; Figure 1b). For each experiment, the lab fault was sheared for 35 mm and shear unload-reload cycles were performed at ~2 mm and ~4 mm to measure the effective

loading stiffness (*Shreedharan et al., 2019*) and to accelerate shear localization (*Frye and Marone, 2002*).

Acoustic Transmissivity Calculations

The raw amplitudes are converted to Acoustic Transmissivity (AT) values, following previous works (*Nagata et al., 2008; Kilgore et al., 2017*). Here, acoustic transmissivity, |T|, is the ratio of the amplitude through the DDS configuration (A_{DDS}) to the amplitude through an intact block (A_{Intact}) having the same length dimension (Equation 2).

$$|T| = \sqrt{\frac{A_{DDS}}{A_{Intact}}} \quad (2)$$

This ensures that the reported values are free from bulk deformation effects. Because each ultrasonic pulse passes through two frictional interfaces, we compute the square root of the amplitude ratio to estimate AT through a single interface (*Nagata et al., 2008*). A_{intact} in our experiments was estimated to be ~29400 bits.

Table S1. List of experiments used in this study with relevant boundary conditions. All experiments were conducted at 100% RH and room temperature of 23 – 25 ^{o}C.

Experiment name	Normal stress (MPa)	Loading velocity (μm/s)	Spring cross-sectional area (cm^2)
p5209	13	11	25
p5221	13	11	25
p5268	10	1-121	16
p5269	10	1-121	9
p5270	10	1-121	25
p5271	10	1-121	20.25
p5272	10	1-121	12.25

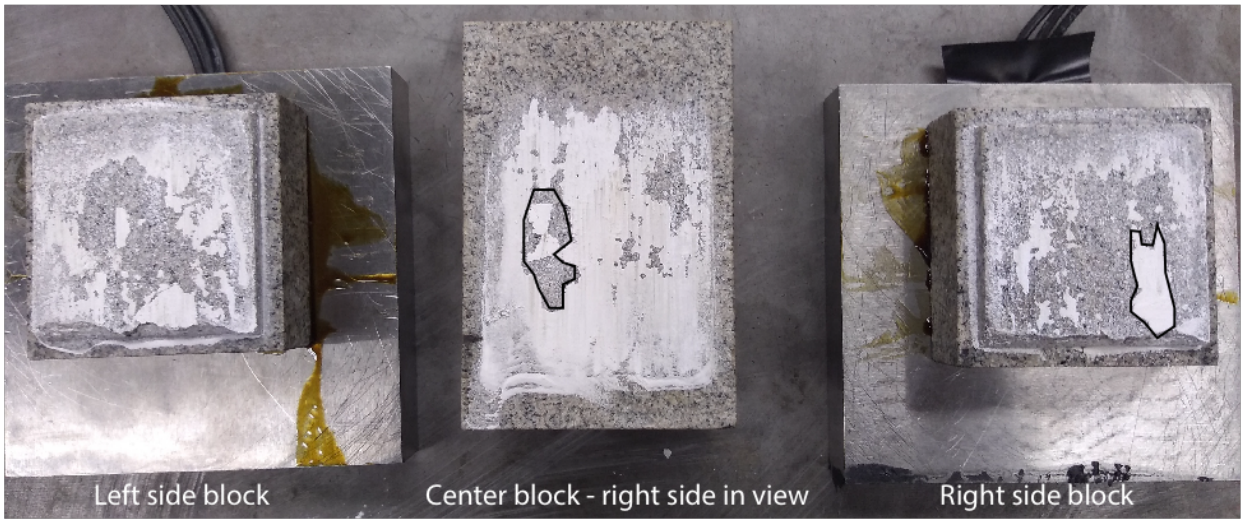

Figure S1. A representative image of the post-shear granular layers sandwiched between rough granite blocks. Note the gouge patches missing in the center block are stuck to the right side block (highlighted in black).

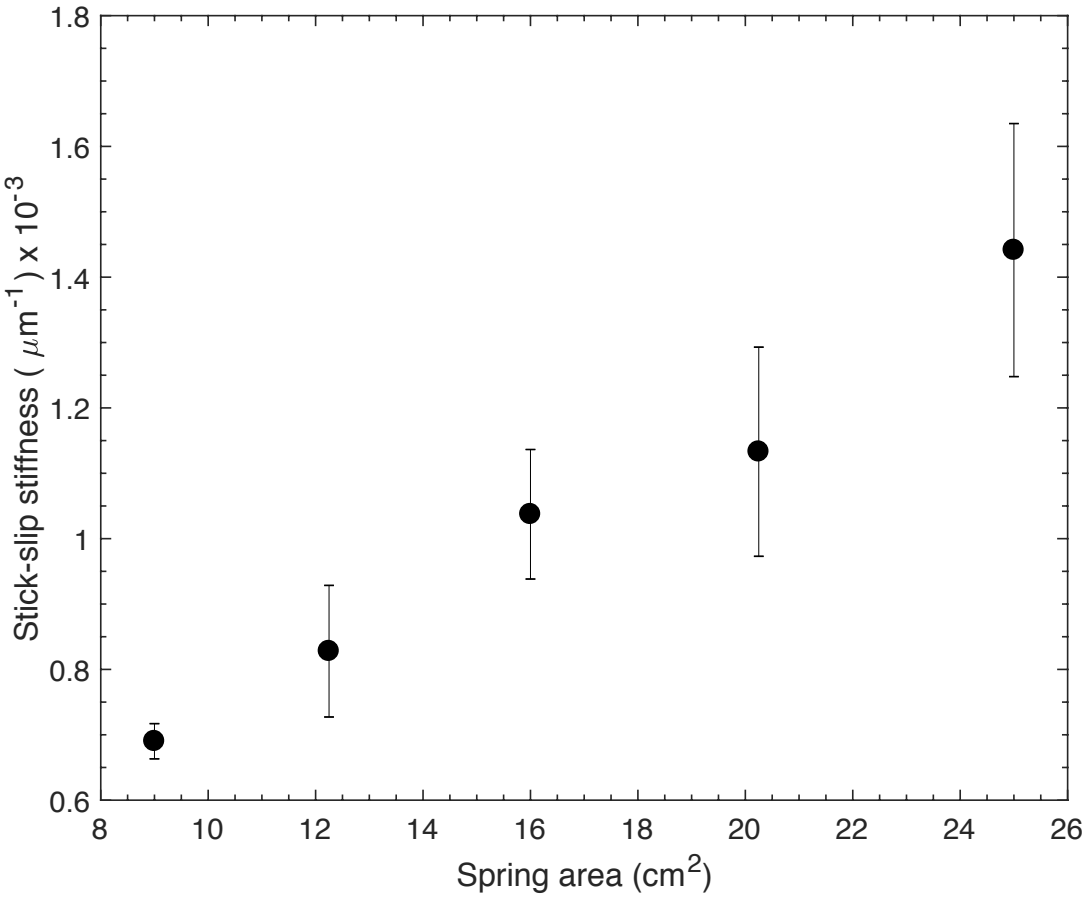

Figure S2. The relationship between spring cross-sectional area and loading stiffness of stick-slip instabilities. Theoretical considerations dictate that, for 1D spring-slider

systems, the loading stiffness is directly proportional to the area and inversely proportional to the length of the spring.

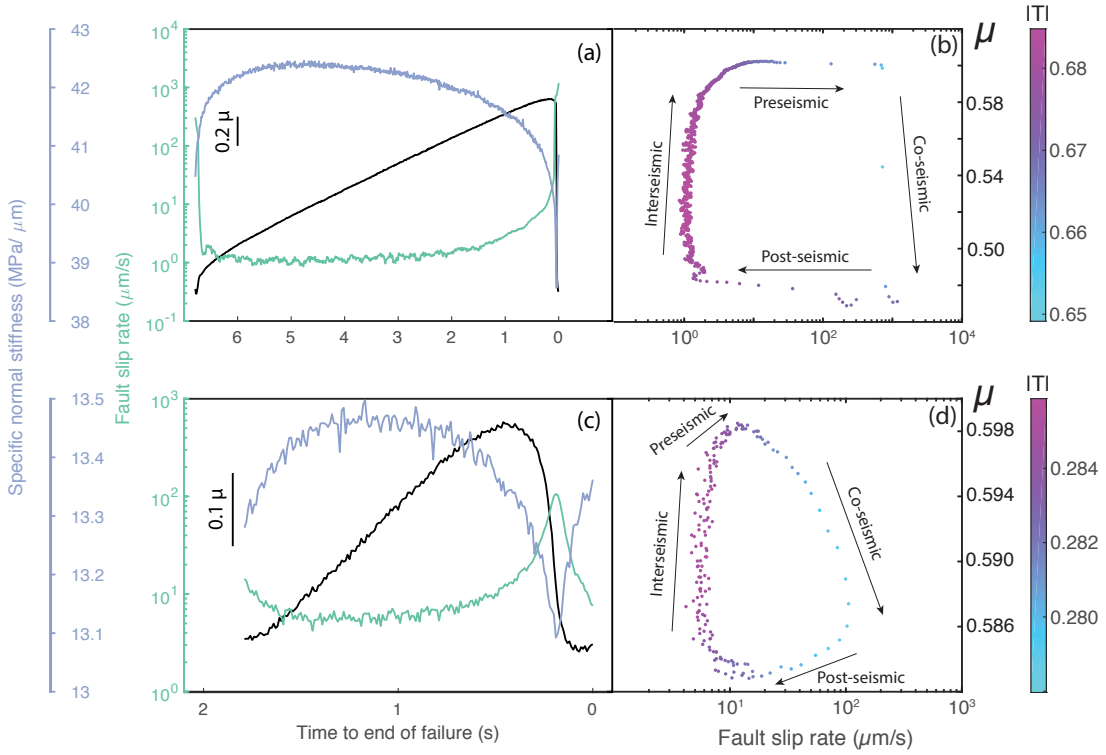

Figure S3. Contact specific normal stiffness calculated from measured ultrasonic transmissivity for representative (a) fast and (b) slow laboratory earthquakes shows preseismic reduction which correlates well with fault slip rate. Phase-plane plots of (a) and (b) are colored by transmissivity values, |T|, for (c) fast and (d) slow earthquakes. Contact specific stiffness was calculated based on methods illustrated in Hedayat et al. (2014) and Kilgore et al. (2017).

References:

1. Frye, K. M., & Marone, C. (2002). The effect of particle dimensionality on granular friction in laboratory shear zones. *Geophysical Research Letters*, *29*(19), 22-1.
2. Gu, J. C., Rice, J. R., Ruina, A. L., & Simon, T. T. (1984). Slip motion and stability of a single degree of freedom elastic system with rate and state dependent friction. *Journal of the Mechanics and Physics of Solids*, *32*(3), 167-196.
3. Hedayat, A., Pyrak-Nolte, L. J., & Bobet, A. (2014). Precursors to the shear failure of rock discontinuities. Geophysical Research Letters, 41(15), 5467-5475.
4. Kilgore, B., Beeler, N. M., Lozos, J., & Oglesby, D. (2017). Rock friction under variable normal stress. Journal of Geophysical Research: Solid Earth, 122(9), 7042-7075.
5. Leeman, J. R., Saffer, D. M., Scuderi, M. M., & Marone, C. (2016). Laboratory observations of slow earthquakes and the spectrum of tectonic fault slip modes. *Nature communications*, *7*, 11104.
6. Nagata, K., Nakatani, M., & Yoshida, S. (2008). Monitoring frictional strength with acoustic wave transmission. Geophysical Research Letters, 35(6).

7. Shreedharan, S., Rivière, J., Bhattacharya, P., & Marone, C. (2019). Frictional State Evolution during Normal Stress Perturbations Probed with Ultrasonic Waves. *Journal of Geophysical Research: Solid Earth*.